THE JOURNAL OF PHYSICAL CHEMISTRY B

Article

pubs.acs.org/JPCB

Prototropic Interactions of Pyrimidine Nucleic Acid Bases with Acridine: A Spectroscopic Investigation

Manas Kumar Sarangi, Ankita Mitra, and Samita Basu*

Chemical Sciences Division, Saha Institute of Nuclear Physics, 1/AF, Bidhannagar, Kolkata 700064, India

Supporting Information

ABSTRACT: In this article, we have investigated the interactions of three pyrimidine nucleic acid bases, cytosine (C), thymine (T), and uracil (U) with acridine (Acr), an N-heterocyclic DNA intercalator, through the changes in photophysics of Acr inside SDS micelles. Fluorescence of $AcrH^{+}$* at 478 nm and its lifetime are quenched on addition of C, T, and U, while a concomitant increment of Acr* is observed only with C. However, the relative amplitude of Acr* increases with a simultaneous decrease in $AcrH^{+}$* only with C. The fluorescence quenching of $AcrH^{+}$* is explained by photoinduced electron transfer (PET), while changes in the relative contributions of Acr* and $AcrH^{+}$* with C are due to associated excited-state proton transfer (ESPT). The rate of electron transfer (k_{ET}) is maximum for T, followed by U and C. The associated ESPT from $AcrH^{+}$* is the reason behind the reduced efficiency of PET with C. The lack of proton transfer with T and U as well as the higher k_{ET} for T compared to U are explained by keto−enol tautomerization and subtle changes in the structure and geometry of the pyrimidine bases.

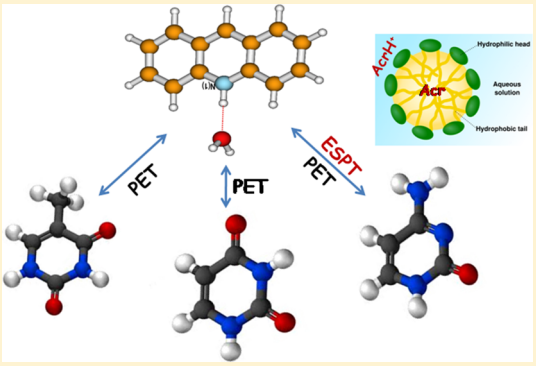

INTRODUCTION

The interaction of nucleic acids with high-energy radiations like UV, X-rays, etc. is of paramount importance since it can lead to radiation-induced damage in DNA with profound consequences like genomic mutation. Despite their large absorption cross sections in the UV region (~260 nm), the building subunits of the nucleic acids, the nucleobases, are relatively photostable due to their efficient ultrafast internal conversion (IC) to the electronic ground state.[1−11] The nucleic acid bases (adenine (A), guanine (G), thymine (T), cytosine (C), uracil (U)), sugars, and phosphate backbone are the prime targets of elementary lesions forming reactive transients by charge (i.e., electron, proton, or hydride) transfer within the strand.[12] To prevent any anticipated cleavage, excess charges from the reactive site migrate preferably over a significant distance by an efficient charge-transfer mechanism in DNA by superexchange or hopping.[13−15] The lowest ionized purine bases (G and A) act as carrier of positive charge (hole) inside oxidized DNA, and the easily reducible pyrimidines bases (C and T) play the role of excess electron carrier in reduced DNA.[16] The above-discussed charge-transfer phenomena inside DNA along with an efficient repair mechanism operate in tandem to prevent lesions from different sources, making DNA robust and faithful as machinery for carrying the genetic information. Among numerous events taking place inside the nucleic acid, photoinduced chemical reactions like excited-state proton transfer (ESPT), photoinduced electron transfer (PET), proton-coupled electron transfer (PCET), H-abstraction, etc. with individual nucleobases and base pairs have gained attention in the past few years. Recent literature reports on electron affinities, ionization energies, and protonation dynamics of individual nucleobases, nucleosides, and base pairs have provided a plethora of information for the predictability of these photoinduced interactions.[13−17] Moreover, significant perturbations in the structures of the nucleobases can dramatically alter the reaction kinetics inside the nucleic acid. Experiments and theoretical calculations from multiple disciplines are being carried out to unravel these photoinduced processes in solutions as well as in gaseous phases.[4−20]

In this article, we have investigated the interactions of three pyrimidine bases C, T, and U and the influence of their subtle structural difference on the photoinduced reaction by probing their interactions with a well-known DNA intercalator acridine (Acr) in SDS micellar media. Although very similar in structure, among C, T, and U, T is found only in DNA, which is replaced by U in RNA. Uracil, for instance, is found in its canonical structure (U1 in Figure 1), a dioxo tautomer, in the Watson−Crick base-pair structure, where it binds to adenine (A) leading to cytotoxic U−A base pair in DNA.[21,22] The presence of U can also arise in DNA from deamination of C and it can be mutagenic. The importance of such an investigation lies in the possibility that mutations may arise from mispairing of the bases in DNA due to occasional appearance of rare tautomers.[22−24] Similarly, protonation and deprotonation at specific sites of the pyrimidines bases become significant in

Received: June 1, 2012
Revised: July 20, 2012
Published: July 20, 2012

   dx.doi.org/10.1021/jp305352b | J. Phys. Chem. B 2012, 116, 10275−10282

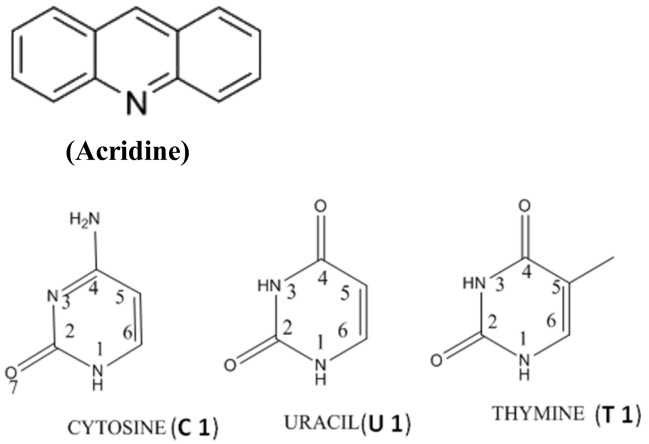

Figure 1. Structures of the chemicals used.

forming hydrogen bonding with their respective purine partners. If the N3 position is protonated, it can interact by hydrogen bonding with a carbonyl or another unprotonated nitrogen (Figure 1). If not protonated, it may interact with protons on the other base.[25] To obtain information on intrinsic properties of these biologically important building blocks, it is of particular interest to study the various photoinduced processes associated with these molecules isolated from their environment. In bulk aqueous solutions, photoinduced processes like PET and ESPT take place at an ultrafast time scale and involve a rapid structural rearrangement of the intervening solvent molecules between donor and acceptor.[26−28] However, the rates of PET and ESPT retard substantially at the interface of biological macromolecules like proteins and DNA as the mobility of the reacting molecules is greatly suppressed due to slower solvation and structural confinement.[29−31] We have chosen the microenvironment of SDS micelles for our study as it resembles the immediate local properties (hydration shell) of different bioaggregates like membranes, protein, DNA, etc.[32]

Acr and its derivatives are the members of the polynuclear N-heteroaromatic family and have a number of significant pharmaceutical uses.[33−35] The interaction of these dyes and its various derivatives with DNA and nucleotides has therefore been studied extensively. There are two modes of binding to DNA: (i) a strong binding site in which the planar ring of Acr is inserted between the planes of the base pairs (intercalation), and (ii) external binding where electrostatic forces play an important role.[34] The excited singlet states of Acr bound to DNA decay via fluorescence and can thus provide important information on the dynamics of the various types of local motions of the DNA molecule on nanosecond time scales. We report herein the prototropic interactions of the individual pyrimidines bases (C, T, and U) with Acr inside SDS micelles. The fluorescence of different Acr derivatives is strongly dependent on the medium, as it is extremely weak in low dielectric solvent like hydrocarbon and becomes moderately strong in aqueous solvent.[36−47] Spectroscopic measurements of excited state pK_a of Acr indicate that, the singlet and triplet states of Acr are stronger bases than the ground state due to large increase in the electron density over the N-atom (pK_a = 5.4, pK_a^* = 9.2).[40,41] Hence, at suitable pH, it abstracts proton from the surrounding solvent and gets protonated ($AcrH^+$). Both Acr and $AcrH^+$ remain in dynamic protonation equilibrium (1) with each other, and show distinct spectroscopic behavior

$$Acr^* + H_3O^+ \leftrightarrow AcrH^{+*} + H_2O \quad (1)$$

However, the photophysics of the tautomeric forms and the protonation equilibrium (1) alter with changes in the local properties like change in pH, dielectric, temperature, etc.[37−45] The sensitivity of Acr to such microenvironmental conditions makes it an effective probe for studying the immediate local properties of its surroundings. By different steady-state and time-resolved measurements, we have tried to investigate the photoinduced interactions of Acr with C, T, and U by monitoring their influences on different photophysical changes of Acr* and $AcrH^+$.

EXPERIMENTAL SECTION

Reagents and Sample Preparation. Acr, C, T, U (Figure 1), and SDS were purchased from Sigma-Aldrich and used without further purification. Water was triply distilled before use. Solutions were prepared by dissolving measured amounts of SDS in triple distilled water (pH = 7) by the volumetric method. All the solutions of Acr, C, T, and U were prepared in 30 mM SDS. The concentration of Acr was kept at 10 μM, and the bases were varied from hundreds of micromoles to a few orders of millimoles. The numbers of Acr molecules per micellar aggregates were calculated to be less than 1; however, the number of quencher molecules per micelle were calculated to be more than 1 (Poisson law).[48,49] The pyrimidine bases are not very well soluble in water; hence, the effective concentration at the SDS interfaces increases substantially. The effective concentration of the bases at the Stern layer is estimated from the literature reports as

$$[Q]_{eff} = \frac{N_{agg}[Q]}{A\{[micelle] - cmc\}} \quad (2)$$

where N_{agg} (~62) is the aggregation number of the micelle, A (~7.43×10^4) is the volume of Stern layers of the micelle, [Q] is the bulk concentration of the bases, and [micelle] = ([surfactant] − [cmc])/aggregation number, where the symbol [ ] denotes the concentration of the individual component.[50,51]

Absorption and Fluorescent Measurements. Steady-state absorption and fluorescence spectra of Acr were recorded by using JASCO V-650 absorption spectrophotometer and Spex Fluoromax-3 spectrofluorimeter, respectively, using a 1.0 cm path length quartz cuvette. For a given sample, the wavelength at which absorbance is maximum (λ_{max}) was used as excitation wavelength for corresponding emission scan. Time-resolved emission spectra of Acr in the absence and presence of pyrimidines were recorded using a picosecond pulsed diode laser based TCSPC fluorescence spectrometer with λ_{ex} ~ 377 nm and MCP-PMT as a detector.[52,53] The emission from the samples was collected at a right angle to the direction of the excitation beam maintaining magic angle polarization (54.7°) with a bandpass of 2 nm. The full width at half-maximum (fwhm) of the instrument response function was 270 ps, and the resolution was 28 ps per channel. The data were fitted to multiexponential functions after deconvolution of the instrument response function by an iterative reconvolution technique using IBH DAS 6.2 data analysis software in which reduced χ^2 and weighted residuals serve as parameters for goodness of fit. All the steady-state and time-resolved measurements were performed at room temperature (298 K).

dx.doi.org/10.1021/jp305352b | J. Phys. Chem. B 2012, 116, 10275−10282

Laser Flash Spectroscopy. Transient intermediates were generated with third harmonic (355 nm) output of our nanosecond flash photolysis setup (Applied Photophysics) containing Nd:YAG (Lab series, Model Lab 150, Spectra Physics). A full width half-maximum of the exciting laser was 8 ns. Transient species in solution were monitored through absorption of light from a pulsed xenon lamp (150 W) at right angle to the laser beam. The wavelength from the probe beam was dispersed with a monochromator and detected with a photomultiplier detector (R928). The photomultiplier output was fed into an Agilent Infiniium oscilloscope (DSO8064A, 600 MHz, 4 Gs/s), and the data were transferred to a computer using IYONIX software. The software ORIGIN 7.5 was used for curve fitting. The solid curves were obtained by connecting the points using B-spline option. The samples were deaerated by passing pure argon gas for 20 min prior to each experiment. No degradation of the sample was observed during the experiment.

RESULTS AND DISCUSSION

Literature reports on photophysics of Acr suggest that both the absorption and fluorescence spectra of Acr depend upon the nature of the species formed in their respective ground and excited states. Both Acr and $AcrH^+$ have absorption maxima at 355 nm, with an additional broad region around 380−420 nm for $AcrH^+$. Depending upon the nature of the environment, the fluorescence of Acr* comes around 400−440 nm (QY = 0.02) and that of $AcrH^+$ appears around 475 nm (QY = 0.66).[37−44] A plot of absorption and normalized emission spectra of Acr in 30 mM SDS is presented in Figure 2. The absorption spectrum

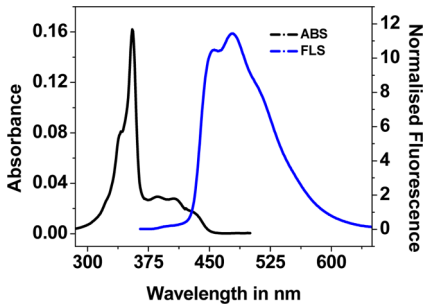

Figure 2. Steady-state absorption and normalized fluorescence spectra (λ_{ex} = 356 nm) of Acr (10 μM) in 30 mM SDS solutions.

shows a maximum at 356 nm with a broad shoulder at the red end 380−420 nm and the emission maximum is at 478 nm. This reflects the presence of protonated species of Acr. Buchviser et al. by steady-state and time-resolved fluorescence reported the formation of $AcrH^+$ inside heterogeneous environment of both SDS micelles and reverse micelles.[44] The formation of $AcrH^+$ at the interfacial hydrophilic region of the SDS micelles and its equilibrium with Acr* have also been reported in the literature.[54] In micellar systems, three domains can be defined: the hydrophilic or aqueous domain, the hydrophobic domain formed by the surfactant alkyl chains, and the micellar interface. As protonation takes place at the interfacial region, $AcrH^+$ is found near Stern layer and Acr is partitioned into the hydrophobic core. The criticality of the distribution of the two species and their respective spectral behavior in presence of the pyrimidine bases have been explored to decipher their protropic behavior and the extent and dynamics of these excited processes inside the SDS micelles.

Interaction of Acr with C, T, and U. For an elaborate study of the photoinduced interaction of Acr with C, T, and U, we used steady-state and time-resolved fluorescence spectroscopic techniques along with laser-flash photolysis.

(a). Fluorescence Quenching of Acr with C. Figure 3a shows a series of representative fluorescence quenching spectra of Acr (λ_{ex} = 356 nm) in the presence of different concentrations of C. With increase in concentration of C, the fluorescence of $AcrH^{+}$* is quenched systematically with the appearance of broad humps at the blue end of each spectrum with an isoemissive point at 435 nm. The hump at the blue end is accredited to the emission from the deprotonated Acr*. The small peak height of Acr* is due to its relatively low fluorescence quantum yield compared to $AcrH^{+}$*.[40−43] It is to be mentioned here that the nature and shape of the corresponding absorption spectra did not show any change in the peak at 356 nm; however, a minute change only around 370−420 nm is observed with addition of C. This infers that there is very little or no interaction with Acr, but, however, a very small scale ground-state interaction between $AcrH^+$ and C is plausible at the interface of SDS micelles. The inset of Figure 3a shows the Stern−Volmer plot for Acr with C is linear with intercept 1.0.[55] The fluorescence quenching of $AcrH^{+}$* along with increase in the emission of Acr* in the presence of C with isoemissive point at 435 nm can be assigned to an ESPT from $AcrH^{+}$* to C. Figure 3b represents the time-resolved decay profiles of Acr (λ_{ex} = 356 nm, λ_{em}= 478 nm) in the absence and presence of varied concentrations of C in 30 mM SDS. The decay curves are biexponential in nature (Table 1) with more than 94% contribution coming from the longer lifetimes of 33 ns, which are quite similar to the earlier reported data in micelles.[44] The longest lifetime (33 ns) is due to the completely protonated species $AcrH^{+}$* and the other is for the excited deprotonated form, Acr*. With gradual addition of C from 0 to 2.2 mM, the lifetime of the protonated species decreases from 33.3 to 25.8 ns, while a very marginal change from 3.6 to 3.0 ns is observed for the deprotonated species. Moreover, the relative amplitude of Acr* increases drastically from 0.04 to 0.3 with a corresponding decrease of that of $AcrH^{+}$*. Both fluorescence quenching and the time-resolved results can be explained as follows. As protonation takes place in the Stern layer of micelles, the $AcrH^{+}$* is found to be at the SDS−water interface. Similarly, due to poor solubility of C in aqueous media, C is expected to be inside the interface of the hydrophobic region of the micelles. As both $AcrH^{+}$* and C are found close to each other near the interface, the collisional probability between two increases substantially with increase in concentration of C. This resulted in substantial quenching of the lifetime of $AcrH^{+}$*, while a negligible change in lifetime is observed for Acr at the core. The steady-state and time-resolved fluorescence quenching of $AcrH^{+}$* with addition of C depicting simultaneous enhancement of fluorescence and relative amplitude of Acr* substantiate ESPT from $AcrH^{+}$* to C via the linked interfacial water ($AcrH^+$−H_2O−C). The ESPT occurs not by the diffusion of free protons but is envisioned as a process propelled by cleavage and formation of H-bond between the donor and acceptor.[56,57] As proton transfer requires an intervening aqueous medium, ESPT between $AcrH^+$−H_2O−C takes place at the interface of the SDS micelle, where the bound water serves as a linker for transfer of hydronium ion.[26−28]

dx.doi.org/10.1021/jp305352b | J. Phys. Chem. B 2012, 116, 10275−10282

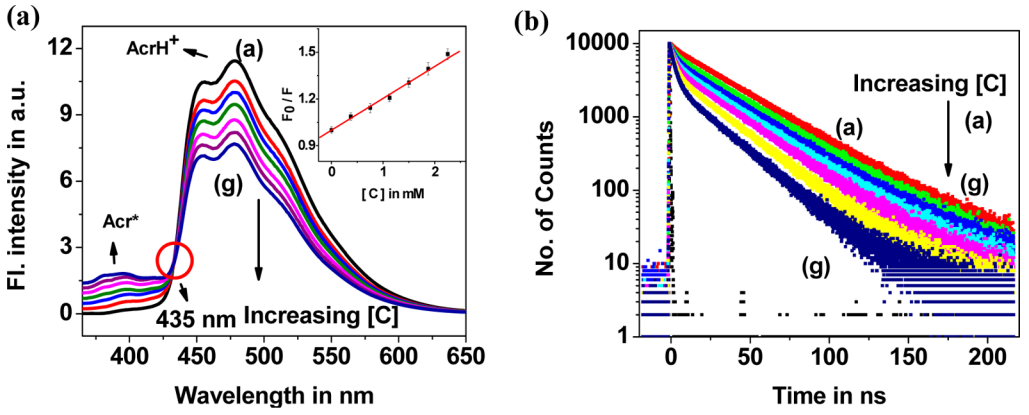

Figure 3. (a) Fluorescence quenching of Acr (10 μM) with increasing concentrations of C (λ_{ex} = 356 nm) from 0 to 2.25 mM with an isoemissive point at 435 nm. The inset in the right shows the Stern–Volmer plot (λ_{em} = 478 nm). (b) Time-resolved fluorescence decays of Acr (10 μM) with increasing concentrations of C (a) 0 mM, (b) 0.37 mM, (c) 0.75 mM, (d) 1.12 mM, (e) 1.5 mM, (f) 1.87 mM, and (g) 2.25 mM in 30 mM SDS (λ_{ex} = 377 nm and λ_{em} = 478 nm).

Table 1. Lifetime Data of Acr (1×10^{-5} M) with Cytosine (C), Thymine (T), and Uracil (U) (λ_{ex} = 370 nm and λ_{em} = 478 nm)[a]

	cytosine (C)			thymine (T)			uracil (U)		
$[Q]_{eff}$ (mM)	τ_1	τ_2	χ^2	τ_1	τ_2	χ^2	τ_1	τ_2	χ^2
0	3.6 ± 0.4 (4.6)	33.3 ± 3 (95.4)	1.02	3.6 ± 0.4 (4.6)	33.3 ± 3 (95.4)	1.02	3.6 ± 0.4 (4.6)	33.3 ± 0.3 (95.4)	1.02
0.37	3.3 ± 0.3 (8)	32.6 ± 2 (92)	1.03	3.6 ± 0.3 (4)	28.5 ± 2 (96)	1.07	3.8 ± 0.5 (4.3)	29.6 ± 4 (95.3)	1.08
0.75	3.1 ± 0.3 (12.1)	31.4 ± 3 (87.9)	1.03	3.5 ± 0.3 (5)	24.8 ± 3 (95)	1.11	3.7 ± 0.3 (4.2)	26.8 ± 3 (95.8)	1.04
1.12	3.0 ± 0.3 (17)	30.2 ± 3 (83)	1.08	3.6 ± 0.2 (5.2)	21.2 ± 2 (94.8)	1.07	3.6 ± 0.4 (4.3)	23.6 ± 3 (95.7)	1.07
1.5	3.0 ± 0.2 (21.2)	28.9 ± 2 (78.8)	1.07	3.5 ± 0.3 (6)	18.2 ± 2 (94)	1.07	3.5 ± 0.3 (4.3)	21.9 ± 2 (95.7)	1.05
1.87	3.0 ± 0.3 (25.5)	27.5 ± 3 (74.5)	1.07	3.5 ± 0.3 (6.1)	16.8 ± 3 (93.9)	1.11	3.4 ± 0.3 (4.4)	18.5 ± 3 (95.6)	1.11
2.25	3.0 ± 0.4 (30)	25.8 ± 3 (70)	1.08	3.6 ± 0.4 (5.8)	14.3 ± 2 (93.2)	1.08	3.4 ± 0.4 (4.3)	16.2 ± 2 (95.7)	1.05

[a]The units of lifetime and concentration of the quenchers are in nanoseconds and millimoles, respectively. The percentage of relative amplitude is given in parentheses.

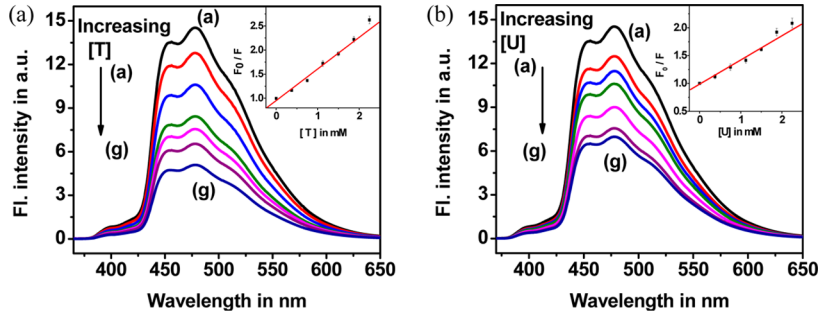

Figure 4. Fluorescence (λ_{ex} = 356 nm) quenching of Acr (10 μM) with increasing concentrations of T (a) and U (b) from 0 to 2.25 mM. The insets of the respective panels show the corresponding Stern–Volmer plots (λ_{em} = 478 nm).

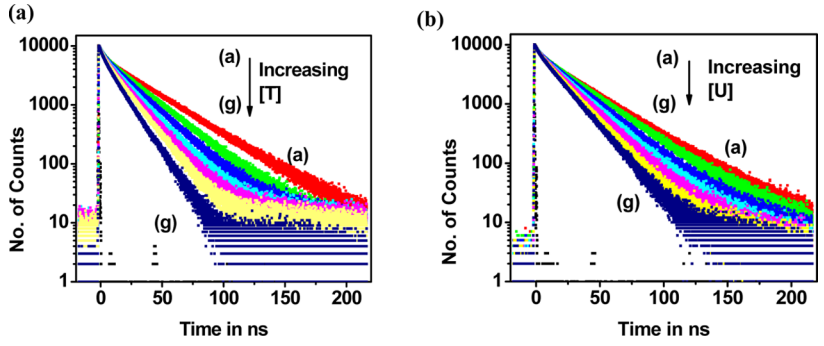

Figure 5. Time-resolved fluorescence decays of Acr (10 μM) of T (a) and U (b) in 30 mM SDS. The concentration of T and U varies as (a) 0 mM, (b) 0.37 mM, (c) 0.75 mM, (d) 1.12 mM, (e) 1.5 mM, (f) 1.87 mM, and (g) 2.25 mM (λ_{ex} = 377 nm and λ_{em} = 478 nm).

dx.doi.org/10.1021/jp305352b | J. Phys. Chem. B 2012, 116, 10275–10282

(b). Fluorescence Quenching with T and U. Unlike C, the absorption spectra of Acr in presence of T and U did not show any change in their corresponding absorption spectrum ruling out any ground-state interaction. However, the fluorescence spectra (λ_{ex} = 356 nm) of $AcrH^+$* at 478 nm is substantially quenched in the presence of T and U (Figure 4a,b). The nature and shape of the emission spectra of Acr remain intact even with the maximum concentration of both T and U, ruling out the possibility of the formation of any excited-state complex. We have not observed any enhancement in fluorescence at the blue end of the spectra of Acr with increase in concentration of T or U, which reflects that the nature of excited-state interactions of Acr with these bases is quite different from that with C as discussed earlier. This difference in interactions might be due to subtle changes in the structures and geometries of the individual pyrimidine bases. The insets in panels a and b of Figure 4 show S−V plots for Acr with T and U, respectively, which are straight lines with intercept 1.0. Figure 5, a and b, represents the time-resolved decay profiles of $AcrH^+$* excited at 377 nm in the absence and presence of varied concentrations of T and U in 30 mM SDS solution. The decay curves are biexponential in nature with most of the contribution coming from $AcrH^+$*. With equimolar addition of the bases T and U, the lifetime of $AcrH^+$* is quenched from 33.3 to 14.3 ns and 16.2 ns, respectively. However the lifetime and amplitude of Acr* remain almost unaltered with addition of the bases. This is explained on the basis of PET from the bases to $AcrH^+$*. Due to protonation at the interface, $AcrH^+$ is found to be close to the interfacial region. Moreover, due to poor solubility in aqueous environment, T and U are also found near the interface. This increases the rate of dynamic quenching of $AcrH^+$* as the encounter probability between $AcrH^+$* and T or U is enhanced due to confined localization. This leads to an effective quenching of the fluorescence lifetime of $AcrH^+$* by both T and U. The relative amplitudes of the two species remain almost intact, eliminating any possibility of proton transfer. These time-resolved results of Acr obtained with T and U are quite different from the results for C, which reflect a change in lifetime as well as amplitude in the two forms of Acr substantiating the occurrence of both PET and ESPT with C while PET alone occurs with T and U.

The differences in the mode of interactions of Acr with C, T, and U cannot just be assigned to the mere positioning or accessibility of the donors and acceptors inside the micellar region as all of them are localized in the hydrophilic interfacial region and the partitioning of the species is expected to be same for equimolar concentration of three pyrimidines. The lack of ESPT for T and U with respect to C can be assigned to subtle changes in structure and tautomerization of the pyrimidines. The canonical forms of C adopt an amino-oxo form (C1), while T and U adopt the dioxo forms (T1, U1) to be complementary with the purine counterpart to form the Watson−Crick base pairs.[58] The occurrence of other enolic tautomeric forms of C, T, and U is also possible by intramolecular proton transfer.[59−62] The proton affinity of C is 227 kcal/mol, while T and U are 210.5 and 208.6 kcal/mol, respectively. Wu et al. reported ab initio and high-pressure mass spectrometric studies of tautomerization of nucleic acid bases with ammonia and calculated the interaction energy of neutral C, T, and U with NH_4^+ as 44.7, 32.8, and 28.6 kcal mol^{-1}, respectively.[61] In case of C, they reported the presence of two stable forms of protonated C, CH1 and CH2, as shown in Scheme 1 with comparable amounts, which can be easily

Scheme 1. Tautomerization between the Two Most Stable Forms of Protonated Cytosine CH1 and CH2

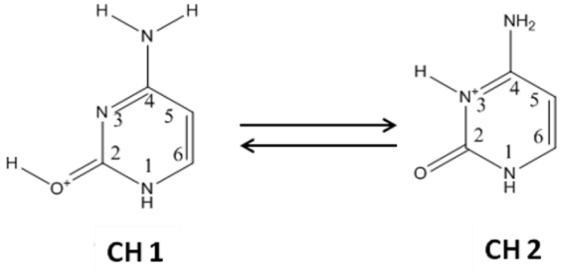

generated from its most stable neutral oxo-amino form without any potential barrier. However, for T and U, in spite of having similar structure and proton affinity, the most stable protonated forms, TH1 and UH1, as in Scheme 2 cannot be readily

Scheme 2. Most Stable Form of Protonated Thymine (TH1) and Uracil (UH1)

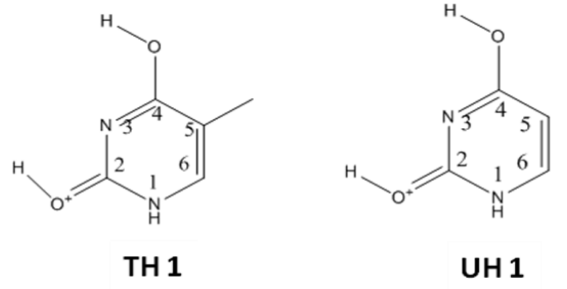

obtained from their stable neutral counterparts T1 and U1, as the intramolecular proton transfer isomerization needs to cross a potential barrier. This limits the protonation of T and U with respect to C. Similar observations were reported by Salpin et al. by mid-infrared multiphoton dissociation spectroscopy of protonated pyrimidines.[62] They reported the simultaneous presence of oxo and enolic isomers of protonated C with oxo isomers being the major contributor showing effective keto−enol tautmerism between the two stable forms of C (Scheme 1). For T and U, they reported the enol forms (TH1, UH1) to be the most abundant species with no signals from the oxo tautomers reflecting lack of keto−enol tautomerism within their experimental limitations. Most importantly, the enolic form of T and U could not be directly generated through a proton transfer to the most stable T and U. Moreover, in solution phase the protonation of C has also been reported, whereas experimental work on protonation of T and U in solution is very rare.[63] Our experimental results of deprotonation of Acr* only with C in SDS solutions reiterate the existence of protonated C.

We have observed electron transfer from all the three pyrimidine bases C, T, and U to $AcrH^+$, while an ESPT is observed from $AcrH^+$ only in the presence of C. In this case, both the events are taking place independently and involved with different sets of donors and acceptors pairs. Proton motion from $AcrH^+$ to C via the intervening water molecule ($AcrH^+$−H_2O−C) is expected to be via Grotthous-type proton-hopping mechanism and is a very fast (picosecond) process, whereas electron transfer from the bases to $AcrH^+$ is a slower one (nanosecond phenomenon).[27,28] Confinements of the electron-transfer probe inside the hydrophobic zones of the micelles

dx.doi.org/10.1021/jp305352b | J. Phys. Chem. B 2012, 116, 10275−10282

make the electron transfer even more sluggish as the collisional probability between the donor and acceptor will be hindered, whereas ESPT between $AcrH^+-H_2O-C$ will be unaffected as the complex is formed near the hydrophilic head groups of the micelles. In our TCSPC setup we are using pulsed laser with fwhm of IRF nearly 270 ps. The fluorescence lifetime quenching of $AcrH^+$ in the presence of bases hence will reveal the time constants for the sluggish electron-transfer process and will limits us from directly calculating the fast ESPT process. However, ESPT between $AcrH^+-H_2O-C$ is confirmed from the enhancement of the peak of Acr* with an isoemissive point in the fluorescence spectra (Figure 3a) along with the increment in the relative amplitude of Acr* in the time-resolved study (Table 1) with increase in concentration of C. The rate constant of electron transfer (k_{ET}, which is the rate-limiting process) for the three bases are calculated by eq 3[55]

$$\tau_0/\tau = 1 + \tau_0 K_{ET}[Q]_{eff} \quad (3)$$

where τ_0 and τ denote lifetimes of Acr* in the absence and presence of the quencher Q (pyrimidines). Figure 6 shows the

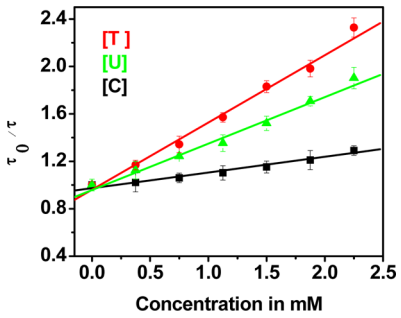

Figure 6. Variation of lifetime of $AcrH^+$ at 478 nm with increasing concentration of C (■), T (red circle), and U (green triangle) from 0 to 2.25 mM DMA.

quenching of lifetime of $AcrH^{+}$* in the presence of the bases at 478 nm. The slopes of the figures divided by the corresponding τ_0 give the respective values of k_{ET}, which are found to be $(0.5 \pm 0.08) \times 10^{10}$, $(1.4 \pm 0.2) \times 10^{10}$, and $(1.2 \pm 0.2) \times 10^{10}$ M^{-1} s^{-1} for C/$AcrH^{+}$*, T/$AcrH^{+}$*, and U/$AcrH^{+}$*, respectively. The relative order of oxidation of the pyrimidines follows the order C > T > U.[16,17] This suggests that the electron-transfer rate should be highest for C and should follow the above trend. However, the values of k_{ET} calculated from the experimental results show that k_{ET} is maximum for T followed by U and C. This discrepancy in the electron-transfer rate of C can be due to its associated proton transfer with $AcrH^{+}$*. We have found a comparison of the rate of electron transfer between C and T in a synthesized DNA sequence in the literature reported by Wagenknecht et al. The C and T are the main electron carriers in DNA, which couple with G and A, respectively, forming the Watson–Crick base pair.[64] They found a significant drop in electron-transfer efficiency with the substitution of a G-C base pair by A-T. They explained this phenomenon by proton-coupled electron-transfer mechanism that influences the G-C base pair more significantly than A-T base pair. Protonation of C radical is a picosecond phenomenon and occurs either from the base pair or from the surrounding water. The authors elaborated that the associated protonation of the C radical limits the electron-transfer efficiency in comparison to T. Moreover, the electron-transfer rate for T is higher than U because of the presence of an electron-donating $-CH_3$ group in T, which increases the electron density over its pyrimidine ring.[65] These observations are in agreement with our time-resolved measurements which reflect a substantial drop in the electron-transfer rate with C which undergoes an ESPT simultaneously.

Transient absorption spectra of Acr with the bases have been studied using the laser flash photolysis technique to identify the transient intermediates formed during the interaction. Panels a, b, and c of Figure 7 display the triplet–triplet (T-T) transient

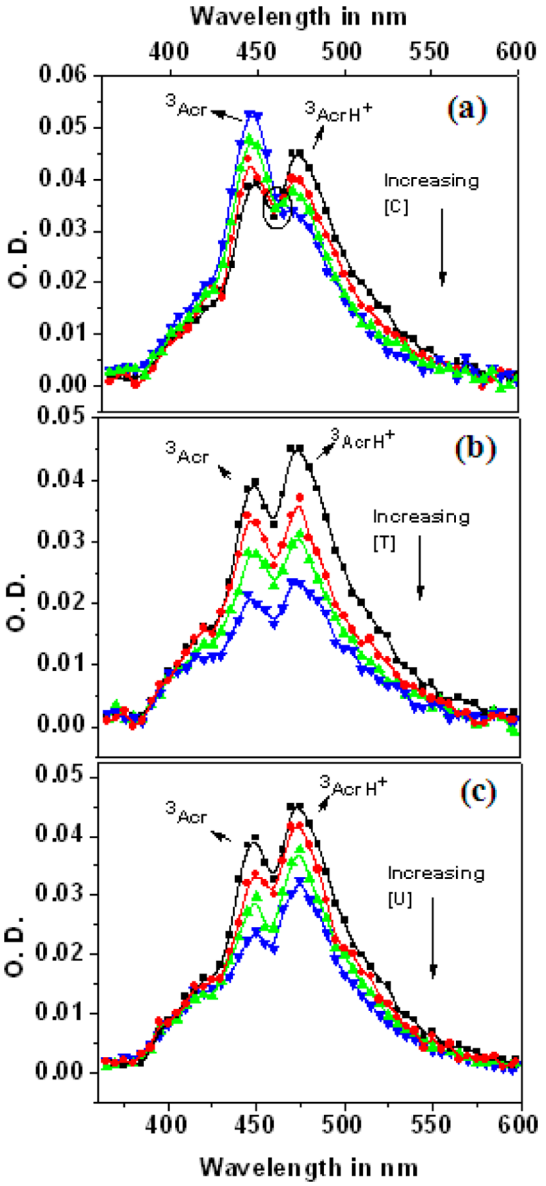

Figure 7. Transient absorption spectra of Acr (10 μM) in 30 mM SDS in the absence (■) and presence of 0.75 mM (red circle), 1.15 mM (green triangle), and 2.25 mM (blue triangle) of C (a), T (b,) and U (c) at 1 μs after the laser flash at 355 nm.

absorption spectra of Acr after 1 μs time delay of the laser flash at 355 nm with varied concentrations of C, T, and U, respectively. T-T absorption spectrum of Acr shows two strong characteristic absorption maxima around 440 and 475 nm.[66–69] The two peaks around 445 and 475 nm are assigned to the absorption of ^{3}Acr and $^3AcrH^+$, respectively. Figure S1 in the Supporting Information shows typical normalized decay

dx.doi.org/10.1021/jp305352b | J. Phys. Chem. B 2012, 116, 10275–10282

profiles for ^{3}Acr and ^{3}AcrH$^+$ at 445 and 475 nm with lifetime of 2.63 and 1.98 μs, respectively. With addition of C, the absorbance at the peak of ^{3}AcrH$^+$ at 475 nm kept decreasing with an increase in the absorbance for ^{3}Acr with peak at 445 nm generating an isosbestic point around 460 nm (Figure 7a). This is evident from the respective decay profiles of ^{3}Acr and ^{3}AcrH$^+$ at 445 and 475 nm. Details of the decay profiles are given in Figure S2A,B in the Supporting Information. The decrease in the absorbance of ^{3}AcrH$^+$ is associated with a decrease in its lifetime from 1.99 to 1.93 μs, while almost no change in lifetime is observed for ^{3}Acr, although its absorbance increases substantially. This explains the selective interaction of C with ^{3}AcrH$^+$ at the surface but not with ^{3}Acr at the core of the SDS micelle. These observations infer the occurrence of ESPT from ^{3}AcrH$^+$ to C, which supports our earlier results as obtained from steady-state and time-resolved fluorescence studies. Figure 8a presents the time-resolved absorption of Acr in presence of

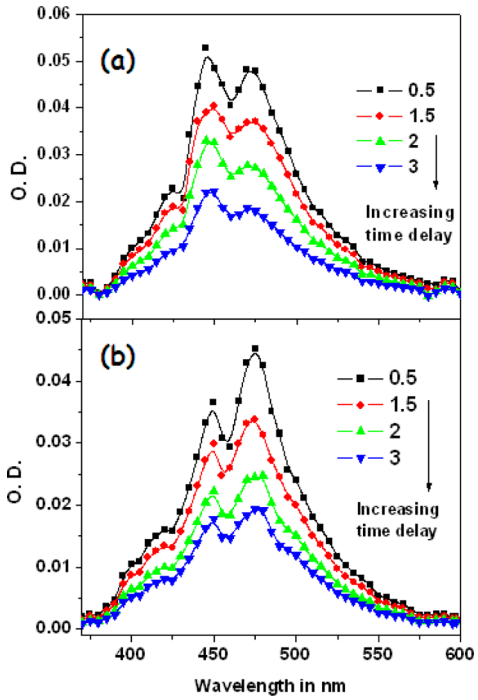

Figure 8. Time-resolved transient absorption spectra of Acr (10 μM) in 30 mM SDS in the presence of 0.75 mM of C (a) and T (b) at 0.5, 1.5, 2, and 3 μs after the laser flash at 355 nm.

1.5 mM of C in 30 mM SDS solution with increasing time delay from 0.5 to 3 μs. The spectra reflect that the hump around 480 nm persists beyond a time delay of 3 μs, indicating the presence of some other component as ^{3}AcrH$^+$ decays much faster compared to ^{3}Acr. This is due to the simultaneous absorption of ^{3}AcrH$^+$ and its corresponding reduced component ^{3}AcrH$^\bullet$, generated through electron transfer from C to AcrH$^+$. The absorption maximum of AcrH$^\bullet$ is around 470 - 500 nm which overlaps with that of ^{3}AcrH$^+$.[69] Therefore, any significant change in this region has not been observed since AcrH$^\bullet$ is formed in expense of ^{3}AcrH$^+$. These observations reflect an associated electron and proton transfer between the excited state AcrH$^+$ and C. With equimolar addition of T and U, the T-T absorption spectra of Acr show a quenching of the both ^{3}Acr and ^{3}AcrH$^+$ at 445 and 475 nm (Figure 7b,c). The corresponding decay profiles and the lifetimes of the corresponding species at 445 and 475 nm in the presence and absence of T are provided in the Figure S3A,B in the Supporting Information. Unlike C, we have not observed any increase in the absorption of ^{3}Acr at 445 nm for both T and U, discarding any deprotonation of ^{3}AcrH$^+$ in the presence of these bases. An overall quenching in absorbance of both ^{3}Acr and ^{3}AcrH$^+$ is observed with addition of T; however, the lifetime of ^{3}AcrH$^+$ at 475 nm decreases from nearly 2 to 1.91 μs due to an electron transfer from the base to ^{3}AcrH$^+$. The time-resolved absorption spectra of Acr in presence of 1.5 mM of T show a persistent hump around 480 nm reflecting the transient AcrH$^\bullet$ generated through electron transfer from the base to ^{3}AcrH$^+$ (Figure 8b).[69] Similar observations are also found for U. As the two species, i.e., ^{3}AcrH$^+$ and ^{3}Acr are in equilibrium with each other in the triplet state, we have observed a simultaneous decrease in the absorption for both of them. However, the extent of decrease in peak intensity of T is found to be a little more than that of U. These results are in good agreement with the observations from the steady-state and time-resolved studies.

CONCLUSION

All the three bases, C, T, and U, contain pyrimidines as a core unit; however, the differential substitutions in the core make them vulnerable to various photoexcited interactions like PET, ESPT, PCET, etc. In this article, we have investigated these interactions by monitoring the changes in the dynamic water-assisted protonation equilibrium between Acr* and AcrH$^+$* in the confined environment of SDS micelles with steady-state and time-resolved spectroscopic techniques. Fluorescence of AcrH$^+$* substantially quenched along with the decrease in lifetime is observed for all the three pyrimidines bases, while a concomitant increase in fluorescence of Acr* is obtained only for C. The quenching of AcrH$^+$* is due to PET from the bases, while an increase in the relative amplitude of Acr* involves an associated ESPT between AcrH$^+$* and C. This differential behavior of three bases with Acr in the excited state arises due to an enhanced keto−enol tautomerism of the protonated C supported by its structure (Scheme 1), which lacks T and U. This associated proton transfer is also the cause of the reduced electron-transfer efficiency of C compared to T and U. Moreover, the greater value of k_{ET} for T compared to U is the result of an enhanced electron density in its pyrimidine ring due to the presence of methyl group as one of the substituents. The steady-state and time-resolved fluorescence observations are also well supported by the transient intermediates characterized by laser flash photolysis.

ASSOCIATED CONTENT

Supporting Information

Decay profiles and lifetimes of ^{3}Acr and ^{3}AcrH$^+$ in presence of the pyrimidine bases are provided in Figures S1, S2, and S3, respectively. This material is available free of charge via the Internet at http://pubs.acs.org.

AUTHOR INFORMATION

Corresponding Author

*E-mail: samita.basu@saha.ac.in. Tel.: +91-33-2337-5345. Fax: +91-33-2337-4637.

Notes

The authors declare no competing financial interest.

■ ACKNOWLEDGMENTS

This work has been funded by Chemical and Biophysical Approaches for Understanding of Natural Processes (CBAUNP) project, SINP of the Department of Atomic Energy (DAE), Government of India.

■ REFERENCES

(1) Swiderek, P. *Angew. Chem., Int. Ed.* **2006**, *45*, 4056−4059.
(2) Choi, K. W.; Lee, J. H.; Kim, S. K. *J. Am. Chem. Soc.* **2005**, *127*, 15674−15675.
(3) Burrows, C. J.; Muller, J. G. *Chem. Rev.* **1998**, *98*, 1109−1152.
(4) Crespo-Hernandez, C. E.; Cohen, B.; Hare, P. M.; Kohler, B. *Chem. Rev.* **2004**, *104*, 1977−2022.
(5) Middleton, C. T.; de La Harpe, K.; Su, C.; Law, Y. K.; Crespo-Hernandez, C. E.; Kohler, B. *Annu. Rev. Phys. Chem.* **2009**, *60*, 217−239.
(6) Kang, H.; Lee, K. T.; Jung, B.; Ko, Y. J.; Kim, S. K. *J. Am. Chem. Soc.* **2002**, *124*, 12958−12959.
(7) Peon, J.; Zewail, A. H. *Chem. Phys. Lett.* **2001**, *348*, 255−262.
(8) Broo, A. *J. Phys. Chem. A* **1998**, *102*, 526−531.
(9) Sobolewski, A. L.; Domcke, W.; Dedonder-Lardeuxc, C.; Jouvet, C. *Phys. Chem. Chem. Phys.* **2002**, *4*, 1093−1100.
(10) Kang, H.; Jung, B.; Kim, S. K. *J. Chem. Phys.* **2003**, *118*, 6717−6719.
(11) Cohen, B.; Hare, P. M.; Kohler, B. *J. Am. Chem. Soc.* **2003**, *125*, 13594−13601.
(12) Lyngdoh, R. H. D.; Schaefer, H. F., III *Acc. Chem. Res.* **2009**, *42*, 563−572.
(13) Wagenknecht, H. A. *Nat. Prod. Rep.* **2006**, *23*, 973−1006.
(14) Giese, B. *Annu. Rev. Biochem.* **2002**, *71*, 51−70.
(15) Hall, D. B.; Holmlin, R. E.; Barton, J. K. *Nature* **1996**, *382*, 731−735.
(16) Greenberg, M. M. *Radical and radical ion reactivity in nucleic acids*; Wiley: New York, 2009.
(17) Wagenknecht, H. A. In *Charge Transfer in DNA—From Mechanism to Application*; Wiley-VCH Verlag GmbH & Co. KGaA: Weinheim, Germany, 2005.
(18) Nielsen, S. B.; Solling, T. I. *ChemPhysChem.* **2005**, *6*, 1276−1281.
(19) Crespo-Hernandez, C. E.; Cohen, B.; Kohler, B. *Nature* **2005**, *436*, 1141−1144.
(20) Sarangi, M. K.; Bhattacharyya, D.; Basu., S. *ChemPhysChem* **2012**, *13*, 525−534.
(21) Kavli, B.; Otterlei, M.; Slupphaug, G.; Krokan, H. E. *DNA Repair* **2007**, *6*, 505−516.
(22) Kurinovich., M. A.; Lee, J. K. *J. Am. Chem. Soc.* **2000**, *122*, 6258−6262.
(23) Parker, J. B.; Bianchet, M. A.; Krosky, D. J.; Friedman, J. I.; Amzel, L. M.; Stivers, J. T. *Nature* **2007**, *449*, 433−438.
(24) Seiple, L.; Jaruga, P.; Dizdaroglu, M.; Stivers, J. T. *Nucleic Acids Res.* **2006**, *34*, 140−151.
(25) Saenger, W. *Principles of Nucleic Acid Structure*; Springer-Verlag: New York, 1984; pp 116−133.
(26) Hynes, J. T. *Nature* **1999**, *397*, 565−566.
(27) Mohammed, O. F.; Pines, D.; Dreyer, J.; Pines, E.; Nibbering, E. T. J. *Science* **2005**, *310*, 83−86.
(28) Laage, D.; Hynes, J. T. *Science* **2006**, *311*, 832−835.
(29) Pal, S. K.; Zhao., L.; Zewail, A. H. *Proc. Natl. Acad. Sci. U.S.A.* **2003**, *100*, 8113−8118.
(30) Pal, S. K.; Peon, J.; Zewail, A. H. *Proc. Natl. Acad. Sci. U.S.A.* **2002**, *99*, 1763−1768.
(31) Pal., S. K.; Zewail, A. H. *Chem. Rev.* **2004**, *104*, 2099−2123.
(32) Kalyansundaram, K. *Photochemistry in microheterogenous systems*; Academic: Orlando, FL, 1987.
(33) Denny, W. A. *Curr. Med. Chem.* **2002**, *9*, 1655−1665.
(34) Belmont, P.; Bosson, J.; Godet, T.; Tiano, M. *Anticancer Agents Med. Chem.* **2007**, *7*, 139−169.
(35) Demeunynck, M.; Charmantray, F.; Martelli, A. *Curr. Pharm. Des.* **2001**, *7*, 1703.
(36) Pedzinski, T.; Marciniak., B.; Hug, G. *J. Photochem. Photobiol., A* **2002**, *150*, 21−30.
(37) Diverdi, L. A.; Topp, M. R. *J. Phys. Chem.* **1984**, *88*, 3447−3451.
(38) Ladner, S. J.; Becker, R. S. *J. Phys. Chem.* **1963**, *67*, 2481−2486.
(39) Whitten, D. G.; Lee, Y. J. *J. Am. Chem. Soc.* **1971**, *93*, 961−966.
(40) Ryan, E. T.; Xiang, T.; Johnston., K. P.; Fox, M. A. *J. Phys. Chem. A* **1997**, *101*, 1827−1835.
(41) Encaranacion, I. N.; Arce, R.; Jimenez, M. *J. Phys. Chem. A* **2005**, *109*, 787−797.
(42) Kellmann, A. *J. Phys. Chem.* **1977**, *81*, 1195−1198.
(43) Tokumura, K.; Kikuchi, K.; Koizumi, M. *Bull. Chem. Soc. Jpn.* **1973**, *46*, 1309−1315.
(44) Buchviser, S. F.; Gehlen, M. H. *J. Chem. Soc., Faraday Trans.* **1997**, *93*, 1133−1139.
(45) Schuette, J. M.; Ndou, T. T.; de la Pena, A. M.; Greene, K. L.; Williamson, C. K.; Warner, I. M. *J. Phys. Chem.* **1991**, *95*, 4897−4902.
(46) Schuette, J. M.; Ndou, T. T.; de la Pena, A. M.; Mukundan, S.; Warner, I. M. *J. Am. Chem. Soc.* **1993**, *115*, 292−298.
(47) Medeiros, G. M. M.; Leitão, M. F.; Costa, S. M. B. *J. Photochem. Photobiol. A: Chem* **1993**, *72*, 225−233.
(48) Tachiya, M. *Chem. Phys. Lett.* **1975**, *33*, 289−292.
(49) Tachiya, M. *J. Chem. Phys.* **1982**, *76*, 340.
(50) Kumbhakar, M.; Nath, S.; Mukherjee, T.; Pal, H. *J. Chem. Phys.* **2004**, *120*, 2824−2834.
(51) Weidemaier, K.; Tavernier, H. L.; Fayer, M. D. *J. Phys. Chem. B* **1997**, *101*, 9352−9361.
(52) Connor, D. V. O.; Phillips, D. *Time Correlated Single Photon Counting*; Academic: New York, 1984.
(53) Demas, J. N. *Excited State Lifetime Measurements*; Academic: New York, 1983.
(54) Sarangi, M. K.; Basu, S. *Phys. Chem. Chem. Phys.* **2011**, *13*, 16821−16830.
(55) Lakowicz, J. R. *Principles of Fluorescence Spectroscopy*; Plenum Press: New York, 2006.
(56) Asbury, J. B.; Steinel, T.; Stromberg., C.; Gaffney, K. J.; Piletic, I. R.; Guon., A.; Fayer., M. D. *Phys. Rev. Lett.* **2003**, *91*, 237402−1.
(57) Fayer, M. D.; Levinger., N. C. *Annu. Rev. Anal. Chem.* **2010**, *3*, 89−107.
(58) Watson, J. D.; Crick, F. H. *Nature* **1953**, *171*, 964−967.
(59) Billinghurst, B. E.; Oladepo, S. A.; Loppnow, G. R. *J. Phys. Chem. B* **2009**, *113*, 7392−7397.
(60) Salpin, J. Y.; Guillaumont, S.; Tortajada, J.; MacAleese, L.; Lemaire, J.; Maitre, P. *ChemPhysChem.* **2007**, *8*, 2235−2244.
(61) Wu, R.; McMahon, T. B. *J. Am. Chem. Soc.* **2007**, *129*, 569−580.
(62) Feyer, V.; Plekan, O.; Richter, R.; Coreno, M.; de Simone, M.; Prince, K. C.; Trofimov, A. B.; Zaytseva, I. L.; Schirmer, J. *J. Phys. Chem. A* **2010**, *114*, 10270−10276.
(63) Aleman, C. *Chem. Phys.* **2000**, *253*, 13−19.
(64) Wagner, C.; Wagenknecht, H. A. *Chem.—Eur. J.* **2005**, *11*, 1871−1876.
(65) Bose, A.; Basu, S. *J. Lumin.* **2009**, *129*, 1385−1389.
(66) Oelkrug, D.; Uhl, S.; Wilkinson, F.; Willsher, C. J. *J. Phys. Chem.* **1989**, *93*, 4551−4556.
(67) Periasamy, N. *Chem. Phys. Lett.* **1983**, *99*, 322−325.
(68) Sarangi, M. K.; Basu, S. *Chem. Phys. Lett.* **2011**, *506*, 205−210.
(69) Neta, P. *J. Phys. Chem.* **1979**, *83*, 3096.